THE ASTROPHYSICAL JOURNAL, 434:232–236, 1994 October 10

ENTRAINMENT BY THE JET IN HH 47

JOHN C. RAYMOND,[1] JON A. MORSE,[2] PATRICK HARTIGAN,[3] SALVADOR CURIEL,[1] AND STEVE HEATHCOTE[4]
Received 1994 January 25; accepted 1994 April 15

ABSTRACT

Fabry-Perot images of the HH 47 optical jet show that the velocity decreases from the center toward the edges which is interpreted as evidence for entrainment. Those images can be used to investigate the rate of entrainment required to account for the observed luminosity. Entrainment along the jet can account for only small fractions of the jet mass and the molecular outflow seen in CO. We compare the density, excitation, and velocity structure of the jet with the predictions of viscous entrainment models and models of entrainment by expulsion of jet material by internal shocks, and find that either type of model can explain the general features of the observations.

Subject headings: ISM: individual (HH 47) — ISM: jets and outflows — ISM: kinematics and dynamics

1. INTRODUCTION

The interaction between an astrophysical jet and its surroundings produces optical emission, and entrainment of ambient gas can be especially important to understanding the jet dynamics. The low-excitation emission lines observed from Herbig-Haro jets arise from weak shocks, and various combinations of internal shock modes and shocks associated with the surrounding material have been invoked to explain the observed line excitations and velocities (e.g., Falle, Innes, & Wilson 1987; Blondin, Fryxell, & Königl 1990; Hartigan & Raymond 1993; Stone & Norman 1993; de Gouveia Dal Pino & Benz 1993; Biro & Raga 1994; Bodo et al. 1994).

Strong bipolar outflows from young stars are also observed in molecular lines. It has long been believed that the momentum fluxes of optical jets from young stars are too small to power molecular outflows, but recent estimates of the densities and lifetimes of the optical jets have reopened this question (Chernin & Masson 1991; Raga 1991; Hartigan, Morse, & Raymond 1994). Several theoretical papers have further stimulated investigation of entrainment by presenting different approaches, including (turbulent) viscous momentum transfer (Cantó & Raga 1991), internal shocks which squeeze material out the sides of the jet (Falle & Raga 1993; Stone & Norman 1993), entrainment at the wings of the main bow shock (Masson & Chernin 1993; Raga & Cabrit 1993), or variations in the jet direction (Biro & Raga 1993). On the observational side, velocity splitting and variations from the centers to the edges of jets (Meaburn & Dyson 1987; Solf 1987; Hartigan et al. 1993) and proper motion variations (Eislöffel & Mundt 1994) have been taken as direct evidence for entrainment.

The HH 47 jet is an exceptional target for a study of entrainment. It emerges from a beautiful dark globule (Bok 1978), and the jet is visible all the way from a reflection nebula near the source to the HH 47A bow shock. Still farther out, the HH 47D bow shock envelopes HH 47A, and HH 47C is visible where the counterjet emerges from the western edge of the cloud. These structures are apparent in Figure 1, the [S II] image from Hartigan, Raymond, & Meaburn (1990). The source lies directly south of the bright star at the top of the image, and the jet extends to the NE. The bright blob at the tip of the jet is HH 47A, and the much fainter (in [S II]) structure beyond it is HH 47D.

Because of its brightness, HH 47 was among the earliest objects studied in detail (Dopita, Schwartz, & Evans 1982). Long-slit echelle studies by Meaburn & Dyson (1987) and Hartigan et al. (1990) defined the kinematics, showing the bow shock structure of 47A and 47D and providing estimates of the shock parameters. Subsequently, Fabry-Perot data cubes provided remarkably detailed knowledge of both the HH 47A and HH 47D bow shocks and their associated Mach disks (Morse et al. 1994). In particular, Morse et al. confirm the Hartigan et al. (1990) result that HH 47A is moving into gas which is already moving outward at high velocity. It may be part of the HH 47D wake or a lower velocity portion of the jet itself.

HH 47 also has a bipolar CO outflow. The map by Chernin & Masson (1991) shows a strong redshifted lobe and a truncated blue lobe, which led Masson & Chernin (1993) to consider entrainment by the optical jet. Recently, Zealey, Suters, & Randall (1993) and Eislöffel, Davis, Ray, & Mundt (1994) have presented images of HH 47 in the H_2 2.12 μm line. *IUE* spectra show a UV continuum with H_2 emission bands due to some combination of Lyα fluorescence and collisional excitation (Schwartz 1983; Böhm, Scott, & Solf 1991), linking the optical jet with the molecular gas.

Morse et al. (1994) obtained Fabry-Perot observations of HH 47 and derived the densities, ionization states, shock velocities, and magnetic fields for the HH 47A and HH 47D shocks and Mach disks. Hartigan et al. (1993) used the same data to study the HH 47 jet. They pointed out that the highest speeds are found along the axis of the jet, with Doppler velocities about 100 km s^{-1} smaller along the edges. This velocity structure is accompanied by a change in the intensity ratio of the [S II] doublet to Hα from $\sim$4 at the center to $\sim$1 near the edges. The striking splitting of the jet into two strands in the velocity resolved images and in high spatial resolution images (Reipurth & Heathcote 1991; Eislöffel & Mundt 1994) is interpreted as limb-brightening associated with excitation in the entrainment layer. Our goal in this paper is to measure the radial velocity gradient and luminosity of the jet, estimate the velocities of the shocks which excite it, determine the rate of entrainment, and compare the derived quantities with predictions of theoretical models.

[1] Center for Astrophysics, 60 Garden Street, Cambridge, MA 02138.
[2] Space Telescope Science Institute, 3700 San Martin Drive, Baltimore, MD 21218.
[3] Five College Astronomy Dept, University of Massachusetts, Amherst, MA 01003.
[4] Cerro Tololo Inter-American Observatory, Casilla 603, La Serena, Chille.

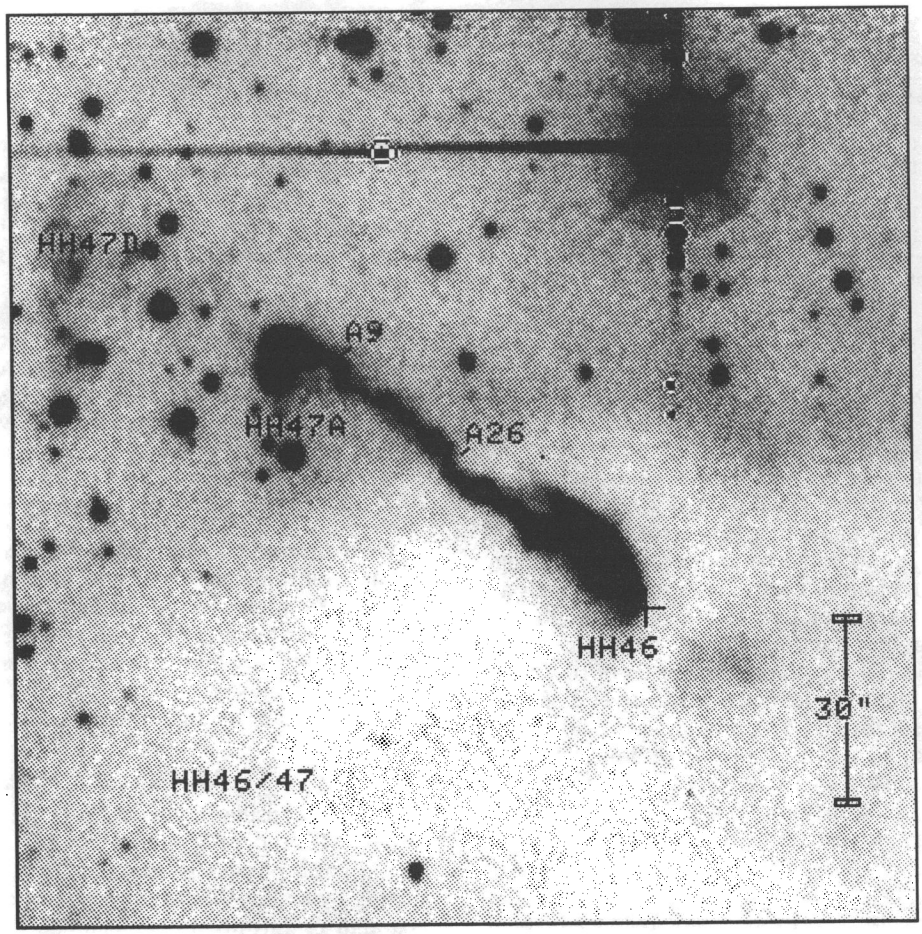

FIG. 1.—Image of HH 47 in [S II] (Hartigan et al. 1990). The knots A9 and A26, which define the region analyzed, are indicated.

2. MEASUREMENTS

We selected the section of the HH 47 jet just behind the HH 47A bow shock for analysis, because this section is relatively straight, and it is free of large scale features which should be analyzed as individual shocks. It extends from just behind the HH 47A bow shock to the kink in the jet about halfway between HH 47A and the source. This section covers knots A9 through A26 in the designation of Reipurth & Heathcote (1991; see also Eislöffel & Mundt 1994). It is 26″ long, or 1.7×10^{17} cm in the plane of the sky, assuming a distance of 450 pc (Reipurth & Heathcote 1991). It is convenient to imagine that the jet consists of concentric cylinders, each having an average velocity, density, and excitation. We use five of the six highest speed images of the Fabry-Perot data shown by Hartigan et al. (1993), each image covering 30 km s^{-1}. There is very faint emission in the -230 km s^{-1} image, but the flux is an order of magnitude smaller than those of the other slices, and its is very uncertain. Doppler velocities closer to rest than -80 km s^{-1} do not appear to be present in the jet itself, though a diffuse region surrounding the jet seems to be present in the -50 km s^{-1} image (Morse et al. 1994). This may be emission from the trailing wings of the HH 47A Bow shock. We are left with the five velocity slices listed in Table 1. From each velocity image, we measured the Hα flux, the [S II] doublet ratio and the [S II]/Hα intensity ratio. The effective radius for each image was taken to be the average FWHM of cuts across the jet. The irregularity of the jet makes the definition of a radius difficult, but the derived radii correspond quite well with the apparent sizes on the images (cf. Eislöffel & Mundt 1994).

Table 2 gives the jet characteristics inferred from the measurements in Table 1. First, we correct for projection into the plane of the sky. The angle between the line-of-sight and the jet has been estimated at 65° (Morse et al. 1994) and 56° (Eislöffel & Mundt 1994). We adopt 60°, giving space velocities twice the Doppler velocities quoted in Table 1, and 2.0×10^{17} cm for the real length of the measured section of the jet. The effective shock velocity, $v_{\rm eff}$, is that which produces the [S II]/Hα ratio according to the models of Hartigan et al. (1994). The total luminosity in each velocity range is based on the 450 pc distance, a reddening of $E(B-V) = 0.18$ (Morse et al. 1993b) and ratios of total to Hα luminosity based on models of low-velocity shocks (Hartigan, Raymond, & Hartmann 1987; Hartigan et al. 1994). The $L/L_{\rm H\alpha}$ ratio decreases from 108 to 75 as $v_{\rm eff}$ increases from 26 to 40 km s^{-1}. The uncertainty in this

TABLE 1

MEASURED PROPERTIES OF HH 47 JET

V_d (km s^{-1})	r_j	6717/6731	[S II]/Hα	$F_{\rm H\alpha}$ (ergs cm^{-1} s^{-1})
−200	1″0	1.34 ± 0.18	4.13	8.9×10^{-15}
−170	1.7	1.24 ± 0.19	2.94	1.6×10^{-14}
−140	2.3	1.21 ± 0.21	1.70	1.8×10^{-14}
−110	2.5	1.20 ± 0.25	1.88	1.5×10^{-14}
−80	2.9	1.12 ± 0.27	1.11	1.2×10^{-15}

TABLE 2

DERIVED PROPERTIES OF HH 47 JET

V^a	r_j^b	v_{eff}^c	n_e^d	L^e	$\langle N \rangle$
−400.....	0.7×10^{16}	26	63	3.5×10^{31}	1200
−340.....	1.2×10^{16}	30	120	5.1×10^{31}	1400
−280.....	1.5×10^{16}	36	160	5.4×10^{31}	1000
−220.....	1.7×10^{16}	34	180	4.7×10^{31}	1300
−160.....	2.0×10^{16}	40	250	3.3×10^{30}	790

[a] Assumes an inclination angle of 60° to line of sight.
[b] Assumes 60° inclination and $d = 450$ pc.
[c] Based on models given in Hartigan et al. 1994.
[d] Electron densities from [S II] diagnostic curves of Czyzak et al. 1986.
[e] Assumes $d = 450$ pc and $E(B-V) = 0.18$.

ratio is smaller than might be expected, because most of the radiation is hydrogen Lyα or two-photon continuum, and these are clearly related to the Hα flux. A 5 km s^{-1} error in shock velocity corresponds to about a 15% error in the conversion factor. The $L/L_{H\alpha}$ ratio could be underestimated if a significant number of Lyβ photons escape, because the models all assume complete conversion of Lyβ to Hα plus two photon continuum. The escaping fraction should be quite small, however, as the Lyβ mean free path is on the order of 10^{10} cm.

We also need to estimate the jet density. Morse et al. (1994) analyzed the structure of the HH 47A bow shock based on the same Fabry-Perot data we use here. From the bow shock Hα luminosity and the 60 km s^{-1} shock velocity derived from both line ratios and line profiles, they found a preshock density of 1020 ± 400 cm^{-3}. They also estimated the jet shock velocity of the Mach disk to be about 90 km s^{-1} based on the [S II]/Hα ratio and the lack of [O II] emission. Ram pressure balance (e.g., Meaburn & Dyson 1987; Hartigan 1989) then leads to an estimate of 700 cm^{-3} for the density of jet material entering the Mach disk. However, there is molecular emission from HH 47 (Schwartz 1981; Böhm et al. 1991; Zealey et al. 1993; Eislöffel et al. 1994) which seems to be very strongly localized at the tip of HH 47, and probably originates in the bow shock. The energy lost to molecular cooling reduces the shock temperature for a given shock velocity, so that the optical emission spectrum resembles that of a slower shock (McKee & Hollenbach 1980; Curiel & Raymond 1994). If the gas ahead of HH 47A is fully molecular, the true bow shock velocity is around 75 km s^{-1}, leading to a revised jet density of 900 ± 400 cm^{-3}.

An alternative density estimate can be derived from the electron density measured from the [S II] doublet ratio and the ionization state and shock compression derived from the [S II]/Hα intensity ratio (Hartigan et al. 1994). The relatively large values of [S II]/Hα imply very small shock velocities, which in turn imply ionization fractions of only a few percent. To derive specific numbers, we turn to the 20–40 km s^{-1}, weak magnetic field shock models of Hartigan et al. (1994). The [S II]/Hα ratios imply 26–40 km s^{-1} shock velocities. The average density lies somewhere between the preshock density and the density of the compressed shocked gas. Hartigan et al. (1994) suggest taking the geometric mean. Using the compressions from the Hartigan et al. models for low magnetic field shocks, we obtain average densities $\langle N \rangle$ between 800 and 1400 cm^{-3}. The uncertainties on the [S II] doublet ratios are large enough, and the ratios are close enough to the low density limit, that we cannot derive a density gradient. For the B3–B11 section of the jet Hartigan et al. (1994) obtain about 1700 cm^{-3}. If we apply their method to the HH 47 A9-A26 spectrum given by Morse et al. (1993b), all of the line ratios imply shock velocities in the range 45 ± 4 km s^{-1} and ionization fractions 0.10 ± 0.03. Unfortunately, the [S II] doublet ratio lies in the low density limit, so we can only conclude that $n_e \leq 100$ cm^{-3} and $n \leq 1000$ cm^{-3}. The Morse et al. spectrum was obtained under fairly poor seeing conditions and at low dispersion which blends the [S II] lines, and it includes low velocity gas which we do not include in this analysis of the jet. It may include a substantial contribution from the photoionized edge of the parent globule, so the jet density could be underestimated.

All in all, it appears that the average jet density is reasonably constant at a value near 1000 cm^{-3}. The shocks which produce the observed emission probably encounter gas at a density near 300 cm^{-3} and compress it to about 6000 cm^{-3}. We will use 1000 cm^{-3} as an average density for comparison with entrainment models.

3. ANALYSIS

We consider two approaches to entrainment separately; viscous entrainment and entrainment driven by material expelled from the jet by internal shocks. These approaches differ in their pictures of the underlying physics, but not necessarily in their observable consequences. Either can explain the observed luminosity, but somewhat different characteristics are assumed for the gas, and different properties are derived.

3.1. *Viscous Entrainment*

First we consider a viscous mixing layer description. Cantó & Raga (1991) developed this picture for optical HH jets. Some of the basic physics is contained in the studies of turbulent mixing by Kahn (1980) and the textbook case of flow in a pipe (Landau & Lifshitz 1959). The energy dissipated in a cylindrical viscous flow is

$$L = \frac{1}{2}\eta\left(\frac{dv}{dr}\right)^2 \pi r^2 l \qquad (1)$$

where η is the viscosity coefficient, $dv/dr = 240$ km s^{-1}/2×10^{16} cm is the radial velocity gradient, and $\pi r^2 l$ is the cylindrical volume. From the numbers in Table 1 and an assumed average density of about 1000 cm^{-3}, we find that the total luminosity in Table 2 requires a kinematic viscosity $\nu = \eta/\rho$ of about 3×10^{20} cm^2 s^{-1}. This is far higher than the molecular viscosity, but it is a plausible value for a turbulent viscosity $v_t l_t$, with turbulent eddy velocities of a few km s^{-1} and sizes near 10^{15} cm. These values for the turbulent eddy size and velocity agree quite well with the estimates of Cantó & Raga (1991) based on scaling of laboratory experiments. Their Appendix A predicts turbulent velocities near 4 km s^{-1} and length scales near 4×10^{14} cm. This kinematic viscosity estimated also agrees with the general expectation that turbulent flows tend to have Reynolds numbers of order 1000 (e.g., Hartquist & Dyson 1988).

The luminosity implies a rate of mass entrainment. The viscous force on the outer boundary of the cylinder is

$$F = \eta \frac{dv}{dr} 2\pi r l\,, \qquad (2)$$

or roughly 3×10^{25} dyn. This force could accelerate $\dot{M}_E \sim 10^{-8}$ solar masses per year to half the jet velocity or 10^{-7} solar masses per year to the 20 km s^{-1} velocity of the CO outflow (Chernin & Masson 1991). If the section of the jet between the source and knot A26 provides a similar force, about 3% of the

jet material has been entrained, and entrainment at the present rate could account for no more than 0.01 $M_\odot$ of outflowing molecular gas over a 10^5 year protostar lifetime, less than 10% of the mass of the blueshifted lobe derived by Chernin & Masson. If one uses the dynamical age of either the optical or molecular jet, the estimated entrained molecular mass is smaller still.

An alternative to finding the viscosity coefficient which accounts for the luminosity is to follow Cantó & Raga (1991), who used the results of laboratory experiments with jets up to Mach 20 to determine the viscosity coefficient and predict the entrainment rate. The greatest uncertainty in this procedure is probably the extrapolation from nearly adiabatic jet experiments to nearly isothermal conditions in HH object jets. The rate of entrainment depends on the density and sound speed of the surrounding medium, which drives material into the mixing layer with an efficiency factor ϵ. Assuming a jet temperature of 10^4 K, a jet velocity of 400 km s^{-1}, and a jet radius of 2×10^{16} cm, their equation 41 predicts a luminosity of 10^{32} ergs s^{-1}. This is about a factor of 2 smaller than the total luminosity from Table 2, which we consider to be very good agreement. It can be taken as confirmation that their determination of ϵ from laboratory experiments is reliable, at least with the uncertainties in the luminosity and density determinations.

The Cantó & Raga (1991) model predicts an average heating rate and temperature in good agreement with the observations. Two other expectations of the viscous entrainment model are also met. The boundary layer velocity is roughly half the jet velocity, as predicted. Also, dv/dr must approach zero at the jet axis, implying that the excitation (as indicated by the [S II]/Hα ratio) should be lowest near the center of the jet. One expectation is not met. The viscous entrainment picture developed by Cantó & Raga assumes a constant velocity gradient over the viscous boundary layer. While this does not conflict with the apparent velocity versus radius in Table 1, the long slit echelle spectrum of Meaburn & Dyson (1987) shows two separate velocity components, rather than a continuous velocity distribution. Spectra of HH 24 (Solf 1987) and HH 34 (Heathcote & Reipurth 1992) also seem to show distinct velocity components. However, slit placement may be crucial, and further observations would be very valuable. Another potential difficulty is that shocks at least as fast as 30 km s^{-1} are needed to account for the strength of Hα, and this casts doubt on the applicability of the subsonic turbulence model.

While the excellent agreement between the quantitative predictions of the viscous entrainment model and the observations of the HH 47 jet might outweigh the difficulties with the velocity distribution and the assumption of subsonic turbulence, we caution that there is *no* direct evidence for the cascade to smaller scales and dissipation on a molecular scale which are generally meant by the term "turbulence." High-resolution images from *HST* may permit a search for the predicted structure. It should also be kept in mind that there is no direct evidence that the jet is immersed in a low temperature, high density medium in pressure equilibrium with the jet, as is assumed in the Cantó & Raga model.

3.2. *Internal Shocks*

An alternative view is that velocity variations in the jet or Kelvin-Helmholtz instabilities along the jet walls generate internal shocks. Internal shocks in themselves do not create the radial velocity gradient seen in the HH 47 jet. However, the high pressure in the shocked region can expel material out the sides of the jet, where it can shock the surrounding gas, accelerate it to an intermediate velocity, and produce the observed velocity structure. Emission will arise from the internal shocks themselves and from shocks in both the surrounding gas and the expelled gas.

Kelvin-Helmholtz instabilities are also the assumed source of turbulence in the viscous entrainment picture, but the viscous and internal shock approaches differ in the expected amplitude of the velocity variations. Many numerical simulations of the Kelvin-Helmholtz instability have concentrated on adiabatic flows (e.g., Bodo et al. 1994), making detailed comparison with observations difficult. However, Blondin et al. (1990), de Gouveia dal Pino & Benz (1993), Stone & Norman (1993), and Chernin et al. (1994) present two- and three-dimensional models which include radiative cooling. The three-dimensional models show a helical instability which would account for the lack of cylindrical symmetry in HH 47. The Kelvin-Helmholtz instability is suppressed by cooling relative to the instability in adiabatic jet models, and it tends to develop only near the end of the jet in the Blondin et al. and de Gouveia dal Pino and Benz models. The Kelvin-Helmholtz instabilities predict knot velocities on the order of $\frac{1}{2}$ the jet velocity, and these may be excluded by the proper motion observations in the case of HH 47 (Eislöffel & Mundt 1994), which seem to show knot velocities close to the jet velocity. However, if the difference between pattern speed and flow speed reported by Eislöffel & Mundt (1994), can be confirmed, that might argue in favor of some variety of K-H instability. Confirmation of the difference in speeds is extremely important.

The alternative to Kelvin-Helmholtz instability is velocity variations in the jet. Raga & Kofman (1992) explored the knot spacing and luminosity in a variable velocity jet analytically, and subsequent numerical simulations have examined various aspects of the shock formation and appearance (Falle & Raga 1993; Hartigan & Raymond 1993; Stone & Norman 1993). This basic picture can also be combined with variations in the jet direction (Biro & Raga 1994) to enhance the entrainment and produce wiggly jet morphologies. This picture is particularly attractive as an explanation for the HH 47 jet, where the center of the jet shows a very high [S II]/Hα ratio, and lower [S II]/Hα wisps trail from some of the knots (Reipurth & Heathcote 1991). The morphology resembles the models shown by Stone & Norman (1993) if one imagines that cylindrical symmetry is broken. Unfortunately, the FP data do not have the spectral resolution needed to search for the sawtooth velocity structures predicted by Stone and Norman.

In the picture of internal shocks driven by jet velocity variations, the luminosity in the central, high-velocity part of the flow arises from the internal shocks, and only intermediate velocity emission comes from the mixing layer. This is convenient, because only modest velocity variations can have survived the journey from the source to the observed region, and the effective shock velocity in the high-velocity slices is relatively small. The knot spacings should obey $\Delta v/v \leq \Delta z/z$ (e.g., Raga & Kofman 1992). The effective shock velocities estimated from [S II]/Hα in the two high velocity slices are 26 and 30 km s^{-1}, or 0.07 and 0.08v_j. These are consistent with the observed spacing $\Delta z/z \leq 0.1$. The luminosity in the high-velocity slices must now be ascribed to about 15–30 shocks (one shock or a forward-reverse shock pair in each knot) at $v_{\rm eff} \sim 26$–30 km s^{-1} in the $n = 300$ preshock material of the central jet, while the luminosities at intermediate velocities can be attributed to 35–40 km s^{-1} shocks driven into the jet surroundings by

expelled material. Using shock areas corresponding to the radii listed in Table 2, the predicted luminosity of the high velocity slices is $1–2 \times 10^{32}$ ergs s^{-1}, in agreement with the observed 0.9×10^{32} ergs s^{-1}. The predicted intermediate velocity luminosity is also about right for 15 shocks. This suggests that shocks normal to the flow (as opposed to oblique crossing shocks) are quite capable of accounting for the observed luminosity.

A series of 30 km s^{-1} shocks which produce the intermediate velocity luminosity can entrain about 10^{-8} solar masses per year and accelerate this mass to $v_j/2 \sim 200$ km s^{-1}. The mass expulsion required for momentum balance is also about 10^{-8} $M_\odot$ yr^{-1}, and this must be squeezed out by internal shocks. However, the material which is pressurized by internal shocks is not expelled very effectively from the sides of the jet. It loses pressure if the cooling time is less than the flow time, $r_j/c_0 \simeq 10^{10}$ seconds (Falle & Raga 1993). For the n_e and $\langle N \rangle$ given in Table 2, and a temperature of 10^4, K, the cooling time is about one-tenth the flow time. This may not be a serious problem, however. Roughly 3×10^{-8} solar masses per year pass through each of the 15–30 internal shocks, so that only a few percent must be expelled to entrain the required mass. In this picture, the small percentage of internally shocked gas expelled balances the higher shock velocity of the entraining shocks to produce comparable luminosities. However, we may be mistaken in ascribing the -200 and -170 km s^{-1} velocity slices to internal shocks and the remaining emission to entraining shocks. The luminosities from internal shocks and entraining shocks are important diagnostics which can be predicted by numerical simulations.

In summary, the picture of entrainment by material expelled from the jet by internal shocks seems to be consistent with the observed luminosity, density and size of the HH 47 jet. The knotty structure and the trailing Hα wisps strongly resemble some theoretical models (e.g., Stone & Norman 1993), and the existence of separate velocity components is likely to be compatible with this picture. The high [S II]/Hα ratio at the center of the jet, and the change in this ratio with radius are also compatible with the model. However, specific numerical comparisons between internal shock models and the data are made difficult by the dependence of the entrainment and the associated emission on such parameters as the density contrast between the jet and its surroundings, the ratio of the jet radius to the internal shock cooling distance, and the jet velocity variations which drive the internal shocks. There are also variants on the basic model which include changes in the jet direction (Biro & Raga 1994). These have the advantage of explaining the asymmetry of the Hα wisps, but they might predict greater line-of-sight velocity variations along the jet than observed. It is possible that the knots which we interpret as internal shocks caused by variations in v_j could be internal shocks driven by Kelvin-Helmholtz instabilities in the jet (e.g., de Gouveia Dal Pino & Benz 1993; Bodo et al. 1994), but the proper motion measurements of Eislöffel & Mundt (1994) probably rule this out for HH 47 and lead us to prefer the models of velocity variable jets.

4. CONCLUSIONS

Either viscous entrainment or entrainment by material expelled from the sides of the jet can explain the overall luminosity and velocity structure of the HH 47 jet. The viscous model makes specific numerical predictions which agree quite well with the observed values, but it is not obvious that subsonic turbulence is at appropriate description for the apparently shock-heated gas of the HH 47 jet. The entrainment rates derived are too small to explain the molecular outflow so if the optical jet drives the molecular flow, it must transfer momentum at the leading bow shock (Masson & Chernin 1993; Raga & Cabrit 1993), rather than along the length of the jet. This agrees with numerical models which predict strong entrainment along the jet only for relatively small Mach number jets (Chernin et al. 1994). It is not obvious what makes the HH 47 jet bright along such a great length, in contrast to other stellar jets. In the viscous picture it may be related to the modest density contrast between the jet and its surroundings ($\eta \sim 1$, while $\eta \sim 10$ in most other jets; e.g., Morse et al. 1992, 1993a), while in the expulsion picture it may be related to the variations in v_j. Finally, it is not at all obvious what role, if any, the magnetic field plays in collimating the jet, in transferring momentum, or in modifying shock structures.

The authors are indebted to A. Raga for discussions about HH object jets. This work was partially supported by The Research Opportunities Fund of the Smithsonian Institution and ST ScI grant GO-4674.01-92A to the Smithsonian Astrophysics Observatory. J. A. M. has been supported by STScI grants NAGW-2689 and NAGW-3268 to Andrew Wilson.

REFERENCES

Biro, S., & Raga, A. C. 1994, preprint
Blondin, J. M., Fryxell, B. A., & Königl, A. 1990, ApJ, 360, 370
Böhm, K.-H., Scott, D. M., & Solf, J. 1991, ApJ, 371, 248
Bodo, G., Massaglia, S., Ferrari, A., & Trussoni, E. 1994, preprint
Bok, B. J. 1978, PASP, 90, 489
Cantó, J., & Raga, A. C. 1991, ApJ, 372, 646
Chernin, L. M., & Masson, C. R. 1991, ApJ, 383, L93
Chernin, L. M., Masson, C., Gouveia Dal Pino, E. M., & Benz, W. 1994, ApJ, 426, 204
Curiel, S., & Raymond, J. C. 1994, ApJ, submitted
Czyzak, S., Keyes, C., & Aller, L. 1986, ApJS, 61, 159
de Gouveia Dal Pino, E. M., & Benz, W. 1993, ApJ, 410 686
Dopita, M., Schwartz, R. D., & Evans, I. 1982, ApJ, 263, L73
Draine, B. T. 1980, ApJ, 241, 1021
Draine, B. T., & McKee, C. F. 1993, ARA&A, 31, 373
Eislöffel, J., Davis, C. J., Ray, T. P., & Mundt, R. 1994, A&A, in press
Eislöffel, J., & Mundt, R. 1994, A&A, in press
Falle, S. A. E. G., Innes, D., & Wilson, M. J. 1987, MNRAS, 225, 741
Falle, S., & Raga, A. 1993, MNRAS, 261, 573
Hartigan, P. 1990, ApJ, 339, 987
Hartigan, P., Morse, J., Heathcote, S., & Cecil, G. 1993, ApJ, 414, L121
Hartigan, P., Morse, J. A., & Raymond, J. C. 1994, ApJ, in press
Hartigan, P., & Raymond, J. C. 1993, ApJ, 409, 705
Hartigan, P., Raymond, J. C., & Hartmann, L. 1987, ApJ, 316, 323
Hartigan, P., Raymond, J. C., & Meaburn, J. 1990, ApJ, 362, 624
Hartquist, T. W., & Dyson, J. E. 1988, Ap&SS, 144, 615
Heathcote, S., & Reipurth, B. 1992, AJ, 104, 2193.
Hollenbach, D. J., & McKee, C. F. 1989, ApJ, 342, 306
Khan, F. D. 1980, A&A, 83, 303
Landau, L. D., & Lifshitz, E. M. 1959, Fluid Mechanics (London: Pergamon)
Masson, C. R., & Chernin, L. M. 1993, ApJ, 414, 230
McKee, C. F., & Hollenbach, D. J. 1980, ARA&A, 18, 219
Meaburn, J., & Dyson, J. E. 1987, MNRAS, 225, 863
Morse, J. A., Hartigan, P., Cecil, G., Heathcote, S. R., & Raymond, J. C. 1993a, ApJ, 410, 764
Morse, J. A., Hartigan, P., Heathcote, S. R., Raymond, J. C., & Cecil, G. 1994, ApJ, 425, 738
Morse, J. A., Heathcote, S., Hartigan, P., & Cecil, G. 1993b, AJ 106, 1133
Raga, A. 1991, AJ, 101, 1472
Raga, A., & Cabrit, S. 1993, A&A, 278, 267
Raga, A. C., & Kofman, L. 1992, ApJ, 386, 222
Reipurth, B., & Heathcote, S. R. 1991, A&A, 246, 511
Schwartz, R. D. 1983, ApJ, 268, L37
Solf, J. 1987, A&A, 184, 322
Stone, J., & Norman, M. 1993, ApJ, 413, 210
Wilking, B. A., Schwartz, R. D., Mundy, L. G., & Schultz, A. B. 1990, AJ, 99, 344
Zealey, W. J., Suters, M. G., & Randall, P. R. 1993, preprint